Reprinted from APPLIED OPTICS, Vol. 20, page 3415, October 1, 1981

Optical fiber index profiles by the refracted-ray method (refracted near-field scanning)

M. Young

This paper has two primary purposes. First, it provides an elementary description and tutorial overview of the refracted-ray method of measuring fiber index profiles. Second, it presents new results concerning the theoretical foundation, the linearity and precision, and other aspects of the method. In particular, we find that index differences may be measured to 5% or better and conclude by showing ~3% agreement with another laboratory and good agreement with numerical aperture measurements performed by participants in an interlaboratory comparison.

I. Introduction

Roughly a half-dozen methods have been proposed and implemented for determining the refractive-index profile of an optical fiber waveguide. At least half of these will no doubt find use in one or another application.

One of the most promising techniques for a simple high-resolution measurement is known as the refracted near-field scanning method or, more compactly, the refracted-ray method. First proposed and demonstrated by Stewart,[1] the method was further developed by White.[2] In addition, I have analyzed precision and other aspects,[3–5] Saunders has compared his results with other methods,[6] and Reid and Stewart have developed an extremely high-resolution scanner.[7]

The purpose of this paper is to offer an elementary, tutorial description of the refracted-ray method, to describe a particular system for implementing it, to analyze it as a measurement system, to present some exemplary results, and to discuss comparisons with other laboratories.

Much of the detail has been worked out by White.[2] Reference 5 includes some further analysis and additionally expands upon many of White's derivations. This paper summarizes, and I refer the reader to Ref. 5 for specifics. I have also discussed other measurement techniques in Ref. 5; for additional discussion and references, see Refs. 8 and 9.

The author is with U.S. National Bureau of Standards, National Engineering Laboratory, Electromagnetic Technology Division, Boulder, Colorado 80303.

Received 6 May 1981.

II. Near-Field Scanning

Near-field scanning depends on the existence of a local acceptance angle (or numerical aperture) at any point on the entrance face of the fiber.[10] That is, the vertex angle of the cone that can enter the fiber and be guided depends on the refractive index of the core at the point of illumination.

The fact was first exploited by Sladen *et al.*[11,12] This group illuminated the end of a short fiber with a uniform Lambertian source. They scanned the exit face of the fiber with a detector and thereby generated a plot of the output power as a function of position along a diameter of the exit face.

The exact proportionality between the local numerical aperture and the power coupled into the fiber holds only for guided rays. Therefore, Adams *et al.* had to derive correction factors for the leaky-ray contribution to the power that propagates into the fiber.[13,14] With these correction factors they are able to calculate the index profile.

Other workers devised a similar scheme for measuring the index profile.[15,16] Rather than illuminate the entire entrance face of the fiber, they focused a laser beam to a point and observed the total power radiated at the far end of the fiber as a function of the position of the point on the entrance face. This variation of near-field scanning also requires correction for leaky modes; in principle, it differs only slightly from the original technique.[17] In practice, entrance-face scanning may be preferable to exit-face scanning, in part because the entrance-face scan may be calibrated precisely, whereas the exit-face scan yields a relative index profile only.

There is another difficulty with both methods of near-field scanning. This is the problem of making the leaky-mode corrections with confidence. Microbending or slight deviations of the fiber from circularity may

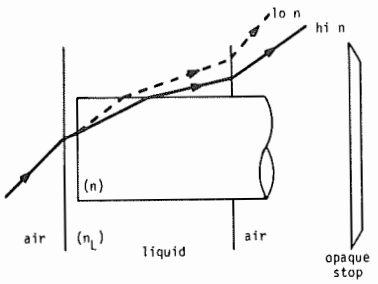

Fig. 1. The lower the index of the fiber, the greater the vertex angle of the emergent cone.

drastically alter the leaky-mode propagation; indeed, Petermann has suggested that the leaky-mode correction may be unnecessary for fibers with nearly square-law profiles.[18] Thus, whereas near-field scanning is both simple and elegant, it may be that its major use will be to give excellent qualitative information about the index profile.

III. Refracted-Ray Scanning

Stewart's innovation was to illuminate a fiber with a focused beam whose vertex angle greatly exceeded the acceptance angle of the fiber and to observe not the rays that are trapped by the fiber but rather the rays that are refracted at the core–cladding interface.[1] With this method, it is in many cases possible to eliminate entirely the deleterious effects of the leaky modes and to develop a system that generates the index profile directly without the need for a correction factor. In addition, refracted-ray scans may be calibrated simply and directly to give quantitative values of refractive index.

To understand the principle of the method, it is helpful to examine Fig. 1. In that figure, a fiber whose refractive index is n is surrounded by a liquid whose index is n_L. The fiber is illuminated by a focused cone of rays; the ray that is drawn in the figure represents the most-extreme meridional ray in the cone. Because the angle of incidence exceeds the acceptance angle of the fiber, the ray is refracted both at the entrance face of the fiber and at the periphery.

Suppose now that we alter the index of the fiber in some way, for example, by changing the fiber entirely. The ray that emerges is now represented by the dashed line in Fig. 1; as the index of the fiber is decreased, the angle formed by the marginal ray's intersection with the axis increases accordingly.

Now we introduce an opaque, circular stop directly behind the fiber; the stop is designed to intercept all but the outermost rays of the emergent hollow cone. A conical shell is transmitted beyond the stop. In the plane of the stop, the inner radius of the shell is always equal to the radius of the stop. The outer radius, however, varies with the index of the fiber. Therefore, the power that is transmitted around the stop also varies with index. The heart of the refracted-ray method lies in the fact that the change of transmitted power is precisely proportional to the change of index.

Figure 1 used a uniform unclad fiber for tutorial purposes. In practice, all that is required is a fiber whose index has no axial variation for the short distance the beam passes through the fiber. For such a fiber, Refs. 2 and 5 show that the angle of refraction θ' from the rear surface of the cell is related implicitly to the refractive index $n(r)$ at radius r through the equation

$$n^2(r) = n_L^2 + \sin^2\theta - \sin^2\theta', \tag{1}$$

where n_L is the index of the liquid in the cell, and $\sin\theta$ is the numerical aperture of the incident cone. The vertex of the cone is scanned across the entrance face of the fiber. If the source is Lambertian, the power radiated into a cone whose vertex angle is θ is proportional to $\sin^2\theta$.[19] Therefore, Eq. (1) may be used to show that the power transmitted beyond the opaque stop is a linear function of $n(r)$.

IV. Radiometric Analysis

In the refracted-ray technique, we insert an opaque stop behind the fiber to block some of the rays refracted by the fiber, as shown in Fig. 1. If the source is Lambertian, the power transmitted beyond the stop may be expressed as

$$P(\theta') = A(\sin^2\theta' - \sin^2\theta_s), \tag{2}$$

where θ_s is the angle subtended by the stop, and A is a constant of proportionality.

If we evaluate A by examining the case where there is no fiber in the cell, we find that

$$2n_L\Delta n(r) = (\sin^2\theta - \sin^2\theta_s)[P(\theta') - P_0]/P_0, \tag{3}$$

where $\Delta n(r) = n(r) - n_L$ and $2n_L\Delta n(r) \cong n^2(r) - n_L^2$. Thus, the power that propagates beyond the stop is almost precisely linear with the index profile of the fiber. (The derivation has been made for guided rays only; see Refs. 2 and 5 and below for a discussion of leaky rays.)

Equation (3) could be used for calibration of the system if the two angles, θ and θ_s, could be measured with sufficient precision. In particular, it is difficult to measure θ_s, because this is the angle subtended by the stop at a point inside the fiber, that is, at the virtual image of the point source as seen from the rear of the cell. In part for this reason, it may be preferable to devise a direct calibration method (see Sec. VIII).

Many sources are not Lambertian. For example, a laser beam that is expanded and passed through a small diameter lens more nearly approximates a uniform point source than a Lambertian source. In contrast, edge emitting diodes and semiconductor lasers emit their radiation more strongly in the forward direction than does a Lambertian source. Such sources can be approximated at least roughly by writing their radiance $L(\theta)$ in the form

$$L(\theta) = L_0\cos^m\theta, \tag{4}$$

where we assume circular symmetry. A Lambertian source is described by $m = 0$ and a uniform point by $m = -1$. Other sources, such as edge emitting diodes, may be approximated by using Eq. (4) with m an integer

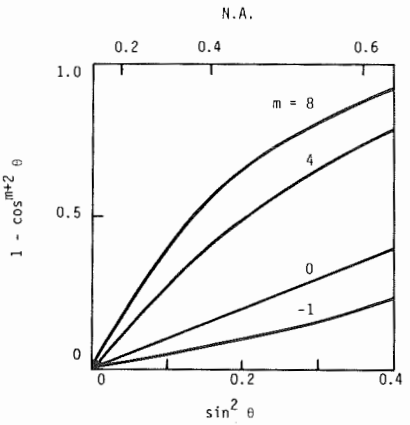

Fig. 2. A function useful for describing the power transmitted by a non-Lambertian source.

between, say, 5 or 10, depending on the specific source. As noted above, the power radiated by a Lambertian source into a cone is proportional to $\sin^2\theta$; see, for example, Eq. (3.17) of Ref. 19. If we follow the derivation leading to that equation but with $L(\theta)$ given by our Eq. (4), we find that the fraction of the total power radiated into a cone is

$$1 - \cos^{m+2}\theta. \tag{5}$$

(This relationship and all subsequent ones are valid when $m = -1$.) Therefore,

$$P(\theta') = A(\cos^{m+2}\theta_s - \cos^{m+2}\theta') \tag{6}$$

in the more general case.

If Eq. (6) is to describe the fiber index profile, it must be linear with $\sin^2\theta'$, because Eq. (3) shows that $\Delta n(r)$ is linear with $\sin^2\theta'$. I have not found it fruitful to try to relate Eq. (6) directly to $\sin^2\theta'$; however, it is instructive to plot $(1 - \cos^{m+2}\theta)$ [Eq. (5)] as a function of $\sin^2\theta$. This is shown in Fig. 2 for several values of m.

The most important curves are those for which m is equal to 0 and -1. The former case is obviously linear, and the latter is nearly so for numerical apertures up to 0.6 or more. Fortunately, what is important is that the curves be linear only over the small range of angles defined by the stop diameter and the numerical aperture of the focusing lens.

As m increases, the curves become less linear. Also, they deviate substantially from the line $m = 0$. Therefore, unless m is precisely 0, a calibration based on Eq. (3) will be invalid.

V. Leaky-Ray Analysis

Suppose that a circular fiber is illuminated off-axis by a focused cone of rays. Geometric optics predicts that certain rays will be trapped by the fiber, whereas certain others will be refracted out of the fiber; we refer to these cases as guided and refracted rays (or bound and radiation modes).

Snyder and his colleagues have shown that some of the rays, although not refracted, in fact suffer high loss and therefore are greatly attenuated after transmission along a relatively short length of fiber; they called these leaky rays.[20–22] The presence of leaky rays renders the guided-ray analysis of Secs. III and IV incomplete.

Adams *et al.* derived correction factors to be used with the near-field scanning technique.[13,14] However, as noted above, there is some doubt as to the utility of these correction factors in some cases. The refracted-ray technique in these cases avoids the necessity for a correction factor by adjusting the angular subtense of the stop so that all the leaky-ray power transmitted by the fiber is intercepted by the stop and only truly refracted rays pass the stop. When the leaky-ray contribution is excluded, the guided-ray analysis is complete.

White has determined the conditions in which leaky rays will propagate beyond the stop.[2] If a fiber has a power-law profile, it is possible to exclude leaky rays, provided that

$$\alpha < 2[(N^2/N_F^2) - 1], \tag{7}$$

where $N_F^2 = 2n^2(0)\Delta$, Δ is the delta parameter of the fiber, N is the numerical aperture of the incident cone, and α is the profile parameter. If $N_F = 0.25$ and $N = 0.5$, $\alpha = 6$; α increases to 10.5 if N_F decreases to 0.2. Thus, leaky rays can be excluded for nearly all practical fibers except possibly step fibers.

A stepped profile may be thought of as a power-law profile for which α approaches infinity. There is no value of θ_s for which leaky rays are completely excluded when α is unbounded. However, White shows that leaky rays may be excluded for all radii beyond

$$r/a < (1 - N_F^2/N^2)^{1/2}, \tag{8}$$

where a is the core radius. This relation is precise only when θ_s has been set equal to the minimum value of θ' and thereby optimized for each fiber. For the examples used above, $r/a = 0.87$ and 0.92, in that order. Beyond these radii, an indeterminate fraction of the leaky-ray power is blocked by the stop; therefore, it is not possible to calculate a correction factor. Thus, the refracted-ray method may not be useful for scanning step fibers beyond about nine-tenths of their radius.

VI. Resolution Limit and Depth of Focus

References 2 and 5 reported that the scanner was diffraction-limited as long as ϵ remained <0.7 or so. Both authors observed a loss of resolution with larger values of ϵ. Although we interpreted our results differently, we assumed that the edge response due to an opaque straightedge adequately described the system.

Stewart[23] has shown that the response of the system to an index step differs from that due to a straightedge. This comes about because the index step has finite thickness; the Fresnel reflection from the boundary between the two dissimilar materials interferes with the directly transmitted wave. Pursuing his argument further, Stewart found that there is a decrease of resolution at values of ϵ smaller than those examined in Refs. 2 and 5.

Using information theory, Stewart showed additionally that resolution is best when the numerical aperture of the opaque stop is a factor of $\sqrt{2}$ less than the numerical aperture of the microscope objective or when ϵ is ~ 0.7.[24] Reid and Stewart have used this result to design a scanner with a numerical aperture of 1.5 and resolution limit of 0.35 μm.[7]

Depth of focus is related to resolution limit and is one factor that may determine the precision with which the end of the fiber must be perpendicular to the axis of the system. For a diffraction-limited optical system such as a microscope objective, depth of focus may be written[25]

$$DF = n\lambda/2(\text{N.A.})^2. \tag{9}$$

If N.A. = 0.5 and λ = 633 nm, the depth of focus DF is ~ 2 μm. If we focus on the center of a 100-μm diam fiber, the edges will be in sharp focus only if the face of the fiber deviates from perpendicularity by less than (2/50) rad or $\sim 2°$.

VII. Apparatus

The experimental apparatus is sketched in Fig. 3. The He–Ne laser beam is expanded by the first microscope objective (MO) and focused by the second 40× microscope objective through a microscope cover slip onto the fiber. The fiber is held in the movable cell whose cross section is shown in Fig. 4 and which is discussed below. The fiber passes through a hole in the opaque stop (OS). The refracted rays escape the fiber and are focused by the condensing lens (CL) onto a uniform, 1-cm diam silicon detector. Because the laser is polarized, the $\lambda/4$ plate is used to reduce the dependence of various reflectances on angle.

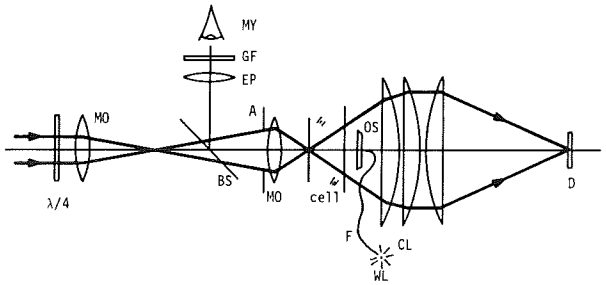

Fig. 3. Experimental setup: Q, quarterwave plate; MO, microscope objective; BS, beam splitter; A, aperture stop; OS, opaque stop; F, fiber; WL, white light source; CL, condensing lens; D, detector; EP, eyepiece; GF, green filter; MY, experimenter. Fiber extends through cell to image plane of MO; see Fig. 4 for detail of cell.

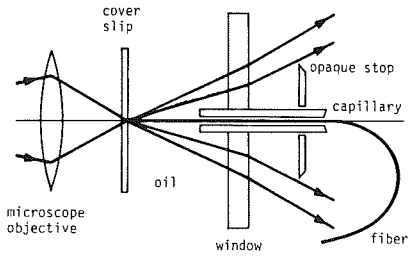

Fig. 4. Detail of cell assembly and focusing optics. Outside the capillary the fiber is confined to the plane perpendicular to the direction of scan.

The condensing lens must have an aperture of $f/1$ or higher. Therefore, it is necessary to design a three- or four-element lens or to use high-aperture Fresnel lenses.[5] Fresnel lenses give substantially greater working distance between the cell and the lens and are preferable from that standpoint. However, some of the data presented here were obtained with a three-element condenser designed from stock plano-convex elements.

The cell is constructed of aluminum. The glass window is fastened with epoxy. The cover slip is fastened to a mounting plate with another epoxy, a fast-setting type that may be removed with a razor blade if the cover slip has to be replaced; the plate is screwed to the cell housing for removal and cleaning. The fiber is introduced through a 0.25-mm capillary tube that is fastened to the window with the same easily removed epoxy, so that the capillary tube may be removed quickly with a heat gun. The outer end of the tube has been formed into a funnel to guide the fiber. The stop is made of aluminum by turning it on a lathe and is fixed in place with piano wire. Stray light that passes through the hole in the stop is intercepted by a black stop fastened to the center of the lens.

In addition, I illuminate the fiber with a white light placed directly behind the cell (or sometimes at the far end) and inspect the entrance face with the beam splitter and eyepiece assembly shown in Fig. 3. The green filter is used to eliminate stray laser light. Once the beam splitter and eyepiece are fixed in place, they may be used to locate the fiber and focus on it by manipulating the cell position. This procedure is accurate to better than 25 μm; I adjust the focus further by scanning across the index dip or other sharp feature and examining the profile for sharpness. The white light source at the far end of the fiber may be replaced with a detector for transmitted near-field scanning.

The system employs a three-axis manipulator whose precision is 2.5 μm (0.0001 in.) or better. Vertical and focusing axes are adjusted by hand, and the horizontal scan is driven with a small ac motor and toothed drive belts.

With one exception, the optical alignment of the apparatus is not critical. The laser beam is introduced by means of two mirrors (not shown). After rough alignment, I center the opaque stop by eye; the aperture stop creates pronounced diffraction rings that make the visual alignment fairly precise. After introducing the condensing lens and positioning the detector by maximizing its output, I use the mirrors to maximize the power through the system; this ensures that the laser beam is centered about the aperture stop that precedes the microscope objective. The opaque stop may be adjusted further at this time, but such adjustment does not seem necessary.

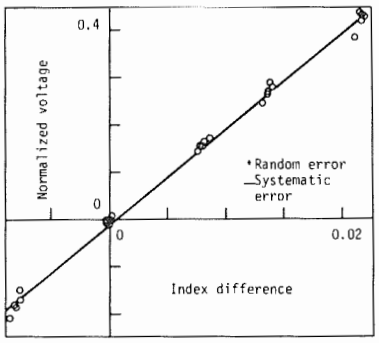

Fig. 5. Normalized voltage as a function of index difference between vitreous silica and oil for a particular stop position. Estimates of random and systematic error are indicated.

The location of the aperture stop, however, is critical. The aperture stop determines the axis of the cone that focuses onto the face of the fiber. If that axis is not very nearly parallel to the axis of the fiber, the scans will be skewed slightly. In a graded-index fiber, the cladding index shows a slight upward or downward slope that is consistently in the same direction on both sides of the core. To correct for this error, the aperture stop must be positioned horizontally to an accuracy of 25 μm or so. With a 40× microscope objective (4-mm focal length), this corresponds to a pointing accuracy of ~6 mrad or one-third of a degree. The adjustment is best made by scanning a fiber repeatedly until the cladding or the oil-index levels on either side of the scan are equalized. In addition, to avoid creating an angular error in the horizontal plane, I introduce the fiber by holding it in place directly above the capillary rather than to one side.

VIII. Calibration

White[2] has calibrated his system by translating the stop to different positions along the axis. I use a somewhat more direct calibration scheme. Ideally, one or more fibers with known core and cladding indices would make calibration an easy matter. Unfortunately, such a set of fibers is not available; neither is there a guarantee that the index of a fiber is precisely that of the preform from which the fiber was drawn.

Malitson has shown that vitreous silica is manufactured with sufficient purity that the index variation from sample to sample or manufacturer to manufacturer is, for our present purposes, negligible.[26] However, Fleming has criticized the use of Malitson's numbers for calculating the index of a fiber; fibers are not annealed but rather are chilled or quenched and may not have the same index as the annealed bulk material.[27,28] Hence, Fleming has measured the index of quenched silica.

At 632.8-nm wavelength, Malitson's and Fleming's Sellmeier equations differ by 0.00028, an amount that is significant when compared with the accuracy to which the indices of the immersion fluids are known. I chose the average value of 1.45719 and assigned an error of ±0.00014.[5]

For calibration, I compared several vitreous silica fibers with each of five oils sequentially. The indices of the oils were supplied by the manufacturer who claimed an accuracy of ±0.0005.[29]

Figure 5 shows a calibration curve. The vertical axis is $(V_q - V_o)/V_o$, where V is the voltage read by the x-y recorder, and q and o stand for quartz (silica) and oil. The horizontal axis is $n_o - n_q$, where n is the index of refraction.

The greatest barrier to a linear calibration may be ensuring the absence of vignetting when the highest-index oil is in the cell (and the emergent cone is largest). It is important to verify the linearity of the system over a large range of indices in case, for example, some of the fibers to be tested have cladding indices significantly less than that of silica. Because of the possibility of vignetting or other effect, an extrapolation may be dangerous if linearity over a sufficient range has not been demonstrated.

Following Natrella, I calculated a line of best fit for the case where both variates have uncertainty; further calculation based on the F test showed linearity to the 99% confidence level.[5,30]

The vertical error bar in Fig. 5 is an estimate of the instrumental limit of error (or resolution) of the x-y recorder; the actual vertical errors are also of this order. The horizontal error is the sum of the index uncertainties just mentioned, as well as an additional ±0.0001 owing to the uncertainty of the oil temperature measurement. Because the large horizontal error bar is not reflected in large vertical scatter, I conclude that most if not all the horizontal error (except the temperature component) is a systematic error that is common to each oil and has approximately constant magnitude and sign; the two horizontal error bars show the random and systematic errors separately (see Table I for a compilation).

When running the unknown sample, I usually choose the oil whose index at 25°C is ~1.464; generally this value is slightly higher than the cladding index, and the values of $\Delta V/V$ for the scan remain within the range defined by Fig. 5. In the unusual event that some of the values fell outside that range, the oil would have to be changed to avoid having to extrapolate the line in Fig. 5.

Table I. Error Budget

Vertical (normalized-voltage units)		
Instrumental limit of error	±0.01	random
Horizontal (refractive-index units)		
Temperature coefficient of refractive index, ±0.25 K	±0.0001	random
Index of vitreous silica	±0.00014	systematic
Index of oils at 25°C	±0.0005	assumed systematic
Subtotals	±0.0001	random
	±0.0004	systematic
Projection of vertical error	±0.0005	random
Totals	±0.0006	random
	±0.0006	systematic

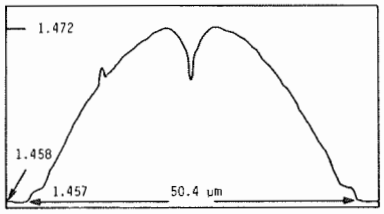

Fig. 6. Refracted-ray scan of fiber *DF-E*. Glitch to left of center is likely due to contamination by dirt or a shard of glass.

After running the scan, I measure the voltage difference corresponding to the core–cladding index difference and compute $\Delta V/V$ for the fiber. The value can be converted directly to index difference by using the slope of the calibration curve of Fig. 5. For relative measurements, it is not necessary to know the precise index of the oil; therefore, Δn should be accurate to ± 0.0006, as detailed in Table I. Because it eliminates the index of the oil from the measurement, this procedure is more accurate than, for example, calibrating each measurement with a quartz fiber and monitoring the temperature of the oil.

The approximate index of the fiber is needed to calculate the numerical aperture, N.A. $= \sqrt{[2n^2(0)\Delta n]}$. However, because n is large, an error in n is not nearly so severe as an error in Δn, and the N.A. may be calculated accurately with only approximate knowledge of the index of the fluid.

IX. Measurements on Actual Fibers

In this section I report the results of refracted-ray scans taken for comparison with numerical aperture measurements by a round robin and with index profile measurements by another laboratory.

Four graded-index fibers designated *DF-A*, *B*, *D*, and *E* had been used in a round robin to intercompare radiation angle or numerical aperture measurements made in each of several laboratories.[31] Figure 6 shows a scan of one of these fibers, *DF-B*. The figure is chosen deliberately to show the glitch to the left of the center, which is probably the result of a speck of dirt or a shard of glass too small to be seen with the eyepiece.

The maximum acceptance angle U for meridional rays is given implicitly by the formula

$$\sin^2 U = n^2(0) - n_c^2, \tag{10}$$

where n_c is the index of the cladding and $\sin U$ is the numerical aperture of the fiber. I measured $n(0)$ and n_c and calculated $\sin U$ from Eq. (10). Table II compares the calculated values with the means of the values obtained for each fiber by the laboratories in the round robin.

In all four cases, the values calculated from index data are equal to or slightly larger than the sample average numerical aperture. The participants in the round robin were instructed to measure the angle between the points at which the intensity was 5% of the peak, whereas the calculated numerical aperture will include all the light transmitted by the fiber. Therefore, we expect the calculated values to exceed slightly the measured values, and this is precisely the case.

I was also fortunate to be able to make an informal comparison with refracted-ray scans by Saunders of Bell Laboratories.[6] We measured the index differences shown in Table III. The other laboratory's value is always slightly higher than that of NBS, but the average difference between our measurements is 3% even though we used different calibration techniques.

Finally, I scanned a step fiber as shown in Fig. 7. The scan reveals a barrier layer, which would not be visible in a conventional near-field scan. Unfortunately, the scan is also marred by ears, or artifacts resulting from the transmission of leaky rays beyond the opaque stop. The arrowheads indicate the region r/a estimated from Eq. (7) to be free of leaky rays; the estimate agrees well with the length of region between the artifacts. The ears may be attentuated significantly by moving the stop axially but at the expense of altering the calibration curve and likely reducing resolution.

Table II. Interlaboratory Comparison of Numerical Apertures

Fiber	Round robin average	Calculated this paper
DF-A	0.235 ± 2.9%[a]	0.264
DF-B	0.163 ± 2.4%	0.174
DF-D	0.202 ± 1.6%	0.208
DF-E	0.195 ± 0.9%	0.202

[a] One standard deviation expressed as percent of mean.

Table III. Interlaboratory Comparison of Index Difference Δn

Fiber	This paper	Other laboratory	Difference (%)
DF-A	0.0237	0.0235	−0.8
DF-B	0.0104	0.0110	+5.8
DF-D	0.0148	0.0156	5.4
DF-E	0.0139	0.0140	0.7
MJ-A	0.0150	0.0154	2.7
MJ-B	0.0156	0.0163	4.5

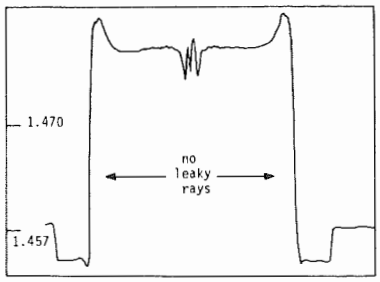

Fig. 7. Refracted-ray scan of step fiber. Arrowheads show region calculated to be free of leaky rays. Artifacts can be diminished by translating stop axially but at the expense of destroying calibration and possibly affecting resolution.

X. Additional Remarks

One of the major practical problems with refracted-ray scanning is the accumulation of dirt particles or shards of glass on the inside of the microscope cover slip. Probably these particles are deposited by the fiber onto the inside of the capillary; they are later picked up by other fibers and deposited in turn onto the cover slip. In any case, such particles accumulate on the cover slip and eventually interfere with the measurement.

The problem may be less severe in a laboratory environment, where relatively few fibers are tested than, say, in a production environment. I simply clean the fibers in acetone after cleaving them; when the cover slip becomes contaminated with particles, I wash or replace it.

K. I. White of the British Post Office informs me that they insert their fibers by using a tube within a tube rather than a single capillary. They push the fiber through a fine tube, cleave it, and place the tube and the fiber in an ultrasonic cleaner (which contains the same oil as the cell). They then withdraw the fiber into the tube and insert that tube into a larger tube that is fixed to the cell. They believe that much of the contamination problem is eliminated in this way.

White further informed me that their cell is cylindrical and mounted in a V-block for easy removal and accurate replacement. Such a design will greatly simplify the removal and cleaning of the cover slip.

Another problem is that the fiber drifts slightly within the cell. The rate of drift varies but is often as large as a micrometer or so per minute. This drift can be arrested by clamping the fiber just outside the cone of refracted rays; because the total motion of the capillary is only 100 μm or so, the clamp need not be fixed to the translation stage. Without this clamping, the fiber sometimes drifts unacceptably before a full scan can be completed.

Although I am the sole author of this article, it has been in certain ways a cooperative venture, and it is my very great pleasure to acknowledge Eric G. Johnson for calculating the edge response of a diffraction-limited annular aperture; Ernest Kim for supplying the exit-face scans; M. J. Saunders of Bell Laboratories, Norcross, Ga., for supplying the excellent data and the fibers with which to compare our results; M. J. Saunders, K. I. White, R. L. Gallawa, and G. W. Day for their very careful and perceptive reviews of Ref. 5; D. L. Franzen for supplying the round robin fibers; Edie DeWeese for her infinite patience preparing the manuscript; and Aaron A. Sanders for providing means, motive, and opportunity.

References

1. W. J. Stewart, A New Technique for Measuring the Refractive Index Profiles of Graded Optical Fibers, in *Technical Digest, IOOC* (IECE, Tokyo, 1977), pp. 395–398.
2. K. I. White, Practical Application of the Refracted Near-Field Technique for the Measurement of Optical Fiber Refractive Index Profiles, Opt. Quantum Electron. **11,** 185 (1979).
3. M. Young, Calibration Technique for Refracted Near-Field Scanning of Optical Fibers, Appl. Opt. **19,** 2479 (1980).
4. M. Young, Linearity and Resolution of Refracted Near-Field Scanning, in *Technical Digest—Symposium on Optical Fiber Measurements*, Natl. Bur. Stand. U.S. Spec. Publ. 597 (1980).
5. M. Young, Refracted-Ray Scanning (Refracted Near-Field Scanning) for Measuring Index Profiles of Optical Fibers, Natl. Bur. Stand. U.S. Tech. Note 1038 (1981).
6. M. J. Saunders, Optical Fiber Profiles Using the Refracted Near-Field Technique: a Comparison with Other Methods, Appl. Opt. **20,** 1645 (1981); M. J. Saunders, Optical Fiber Profiles Using the Refracted Near-Field Technique: A Comparison with Interferometry, *Technical Digest—Symposium on Optical Fiber Measurements, 1980, Digest supplement* (Optical Electronic Metrology Group, U.S. National Bureau of Standards, Boulder, Colo. 80303, 1980); see also Ref. 4 for complete digest.
7. D. C. J. Reid and W. J. Stewart, Ultrahigh Resolution Refractive Near-Field Profiling, in *Technical Digest, Third International Conference IOOC* (Optical Society of America, Washington, D.C., 1981), paper TUG6.
8. D. Marcuse and H. M. Presby, Index Profile Measurements of Fibers and Their Evaluation, Proc. IEEE **68,** 666 (1980).
9. H. M. Presby and D. Marcuse, The Index-Profile Characterization of Fiber Preforms and Drawn Fibers, Proc. IEEE **68,** 1198 (1980).
10. D. Gloge and E. A. J. Marcatili, Multimode Theory of Graded-Core Fibers, Bell Syst. Tech. J. **52,** 1563 (1973).
11. D. N. Payne, F. M. E. Sladen, and M. J. Adams, Index Profile Determination in Graded Index Fibers, in *Proceedings, First Conference on Optical Fibre Communication*, IEE Conf. Publ. London **132,** 43 (1975).
12. D. N. Payne, F. M. E. Sladen, and M. J. Adams, Determination of Optical Fiber Refractive Index Profiles by a Near-Field Scanning Technique, Appl. Phys. Lett. **28,** 255 (1976).
13. M. J. Adams, D. N. Payne, and F. M. E. Sladen, Correction Factors for the Determination of Optical-Fibre Refractive-Index Profiles by the Near-Field Scan Technique, Electron. Lett. **12,** 281 (1976).
14. M. J. Adams, D. N. Payne, and F. M. E. Sladen, Length-Dependent Effects Due to Leaky Modes on Multimode Graded-Index Optical Fibers, Opt. Commun. **17,** 204 (1976).
15. J. A. Arnaud and R. M. deRosier, Novel Technique for Measuring the Index Profile of Optical Fibers, Bell Syst. Tech. J. **55,** 1489 (1976).
16. G. T. Sumner, A New Technique for Refractive Index Profile Measurement in Multimode Optical Fibres, Opt. Quantum Electron. **9,** 79 (1977).
17. For simplicity of nomenclature and for avoiding confusion, I shall refer to both these methods as near-field scanning. When it is necessary to distinguish between them, I shall use the terms entrance-face scanning and exit-face scanning. Likewise, I will not use the somewhat cumbersome term refracted near-field scanning but rather will refer to the refracted-ray method.
18. K. Petermann, Uncertainties of the Leaky Mode Correction for Near-Square-Law Optical Fibers, Electron. Lett. **13,** 513 (1977).
19. M. Young, *Optics and Lasers, An Engineering Physics Approach* (Springer, New York, 1977), Chap. 3.
20. A. W. Snyder, Leaky-Ray Theory of Optical Waveguides of Circular Cross Section, Appl. Phys. **4,** 273 (1974).
21. A. W. Snyder, D. J. Mitchell, and C. Pask, Failure of Geometric Optics for Analysis of Circular Fibers, J. Opt. Soc. Am. **64,** 608 (1974).
22. A. W. Snyder and D. J. Mitchell, Leaky Rays on Circular Optical Fibers, J. Opt. Soc. Am. **64,** 615 (1974).
23. W. J. Stewart, Detail Resolution in Optical Fibre Index Profiling Methods, AGARD Conf. Proc. **219, 28-1**(1977). This work is also expanded in an unpublished paper.

24. W. J. Stewart, Resolution of Near-Field Optical Fiber Refractive Index Profiling Methods, in *Proceedings, International Meeting on Scanned Image Microscopy, London 1980* (Academic, New York, 1981), pp. 233–239.
25. L. C. Martin, *Technical Optics, Vol. 2* (Pitman and Sons, London, 1960), Chap. 3.
26. I. H. Malitson, Interspecimen Comparison of the Refractive Index of Fused Silica, J. Opt. Soc. Am. **55,** 1205 (1965).
27. J. W. Fleming, Material Dispersion of Lightguide Glasses, Electron. Lett. **14,** 326 (1978).
28. J. W. Fleming, Dispersion in Step-Index Silicone-Clad Fibers, Appl. Opt. **18,** 4000 (1979).
29. I am indebted to Michael Liva and William Sacher of Cargille Laboratories for providing the liquids along with their indices, their Sellmeier coefficients, and a statement of accuracy.
30. M. G. Natrella, *Experimental Statistics*, Natl. Bur. Stand. U.S. Handb. 91, 5-22, 5-23, 5-27 (1963).
31. D. L. Franzen and E. M. Kim, Interlaboratory Measurement Comparison to Determine the Radiation Angle (N.A.) of Graded-Index Optical Fibers, Appl. Opt. **20,** 1218 (1981).